Analysis of Current Control Bandwidth in Current Source Type Motor Emulator

Gensui Tanaka[1], Katsuki Miura[1], Keita Ohata[1], Hitoki Watanabe[1], Jun-ichi Itoh[1], and Ikuya Sato[2]
[1] Nagaoka University of Technology, Japan
[2] FUJI ELECTRIC CO., LTD., Japan

***Abstract*-- This paper focus on the stability issue of an inverter test system with a current source type motor emulator (CSTME). The CSTME imitates various motor operations with accuracy. However, the CSTME requires high current control bandwidth to prevent interference between the current controls of both the inverter under test (IUT) and the CSTME. This paper reveals the required current control bandwidth, which is to prevent interference between current controls, based on root locus analysis results. From the result of the stability analysis, the current controller of the CSTME requires 2.2 times higher bandwidth than IUT's bandwidth. The stability limit of the root locus analysis agrees with the simulation of the time domain. In addition, the effect to the stability limit with time delay is also investigated. Then, the CSTME's required current control bandwidth becomes more than 3.1 times of that of IUT. The validity of the analysis is verified by the simulation on the time domain.**

***Index Terms*-- Current control bandwidth, Motor emulator, Root locus, Stability Analysis.**

I. INTRODUCTION

Recently, a Hardware-in-the-loop (HIL) simulation has been used before experimental verification [1]-[3]. The HIL simulation provides some advantages over conventional off-line simulation, such as reliability and shorter development time. The HIL simulation has been mostly used to test the control system, which is called Controller HIL (CHIL) simulation. The CHIL simulation, which receives gate-signal from the controller under test and sends the detected signals, is used to confirm the response and the performance of the system. However, the CHIL simulation tests only the controller, not the hardware for driving motors including power converters and other components.

On the other hand, a Power HIL (PHIL) simulation has been attracted to develop the power converter and its control without an actual load. The most significant advantage of the PHIL simulation is that it can confirm the performance and reliability of the main power circuit, such as power loss, temperature rising, surge voltage, detection circuit accuracy, and so on.

The PHIL simulation is very effective in developing a special specifications motor drive system, such as high speed, high power density and so on. The development of special specifications motor drive system has to prepare an inverter under test (IUT), a motor under test (MUT), a coupling, a load machine, and load machine inverter. Many kinds of equipment are required for the inverter test. Moreover, the development period will be long because there are many development items in not only the IUT but also the MUT and load machine [4]. The PHIL simulation, which emulates the behavior of a test motor to develop a test inverter and controller, is so-called "a motor emulator." The motor emulator reduces the cost, the development time, and the space to build a test environment.

There are two types of motor emulators, the voltage source type [5]-[8] and the current source type [9]-[14]. The voltage source type motor emulator imitates the back electromotive force (EMF) of the target motor and the voltage drop on the inductor and the resistor. However, the voltage source type motor emulator does not apply to the IUT with an open-loop control or a V/f control. In addition, the voltage source type motor emulator does not evaluate the current transients with accuracy even when the current control is implemented in the IUT because it imitates the back EMF and the voltage drop in the steady state. On the other hand, the current source type motor emulator (CSTME) imitates the motor current accurately. The motor current commands are calculated by the terminal voltage of the CSTME. Besides, the CSTME is applied regardless of the control method of the IUT. In addition, many kinds of motors are imitated by changing the motor differential equation implemented in the controller of the CSTME [9]-[11]. For these reasons, the CSTME is more suitable for the motor emulator system in terms of general-purpose use.

However, the control of the CSTME may become unstable because of the interference between the current control bandwidth of both the IUT and the CSTME [13]-[14]. Empirically, the current control bandwidth of the CSTME needs to be larger than that of the IUT. However, it seems that the minimum bandwidth of the CSTME was not clearly mentioned in the past literatures.

This paper clarifies the control bandwidth required for the current control of the CSTME. The stability limit is revealed by the stability analysis with a root locus. The originality of this paper is the evaluation of the bandwidth, which is required to prevent interference between the current controls based on a root locus analysis.

This paper is organized as follows; first, the configuration of the CSTME is introduced; second, the design method of the controller is described; third, a stability analysis of the inverter test system using the CSTME is discussed by a root locus, and the current response required for the CSTME is clarified; Then the validity of the analysis result is confirmed by the simulation.

II. Current Source Type Motor Emulator

Fig.1 shows the system configuration of an inverter test system using the CSTME. The hardware configuration of the CSTME is the same as a PWM rectifier. The controller of the CSTME detects the phase current and the output voltage of the IUT. The virtual motor speed and torque are given by the equation of motion of the motor. The calculated motor speed value is sent to the controller of the IUT.

The state equation of an IPMSM based on the dq-axis is expressed as

$$P\begin{bmatrix} i_d \\ i_q \end{bmatrix} = \begin{bmatrix} -\frac{R}{L_d} & \omega_{re}\frac{L_q}{L_d} \\ -\omega_{re}\frac{L_d}{L_q} & -\frac{R}{L_q} \end{bmatrix}\begin{bmatrix} i_d \\ i_q \end{bmatrix} + \begin{bmatrix} \frac{v_d}{L_d} \\ \frac{v_q}{L_q} \end{bmatrix} + \begin{bmatrix} 0 \\ -\frac{\omega_{re}\psi_m}{L_q} \end{bmatrix} \quad (1),$$

where v_d and v_q are the dq-axis voltage, i_d and i_q are the dq-axis current, R_a is the armature resistance value, L_d and L_q are the dq-axis synchronous inductance values, ω_{re} is the electric angler frequency, P is the differential operator, and Ψ_m is the flux linkage of the permanent magnet. Here, the output torque T_e and the relationship between the electric angular velocity and torque on the dq-axis are expressed as

$$T_e = p\{\psi_m i_q + (L_d - L_q) i_d i_q\} \quad \cdots\cdots (2),$$

$$P\omega_{re} = \frac{P}{J}(T_e - T_L) \quad \cdots\cdots (3),$$

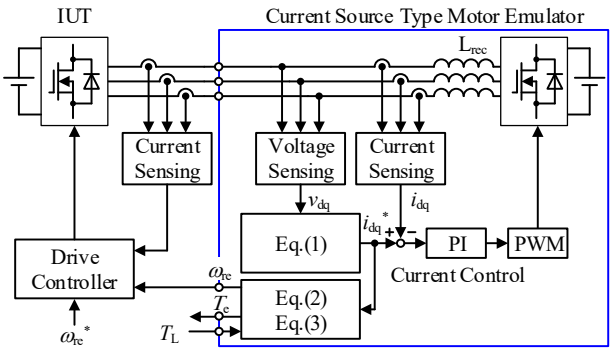

Fig. 1 The system configuration of the inverter test system with current source type motor emulator.

where T_L is the load torque, p is the pairs of poles, and J is the inertia of the motor. It is noted that the damping factor and spring factor are in (3).

The current commands are obtained by solving the differential equation (1), (2), and (3) for the current using the Euler method in a DSP.

Fig. 2 shows the whole system block diagram of the CSTME. The CSTME controller is composed of the motor model and the current controller. The feed-forward compensation is applied in the CSTME controller in order to cancel the interference between the inductor on the dq-axis. The low pass filters, which are connected in front of adding a point, are used to cancel the zero points of the closed-transfer function of the current control.

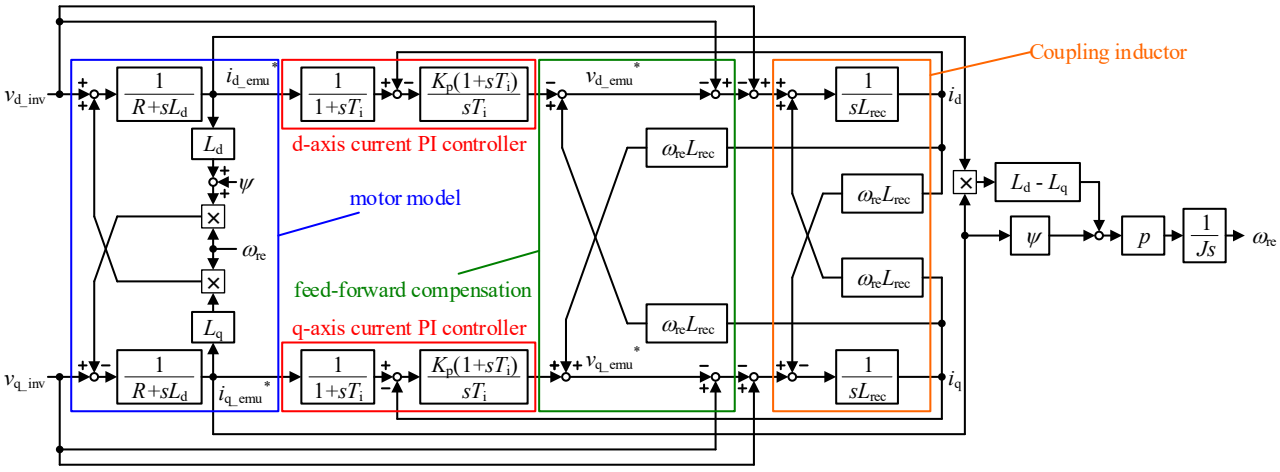

Fig. 2 Control block diagram of the CSTME.

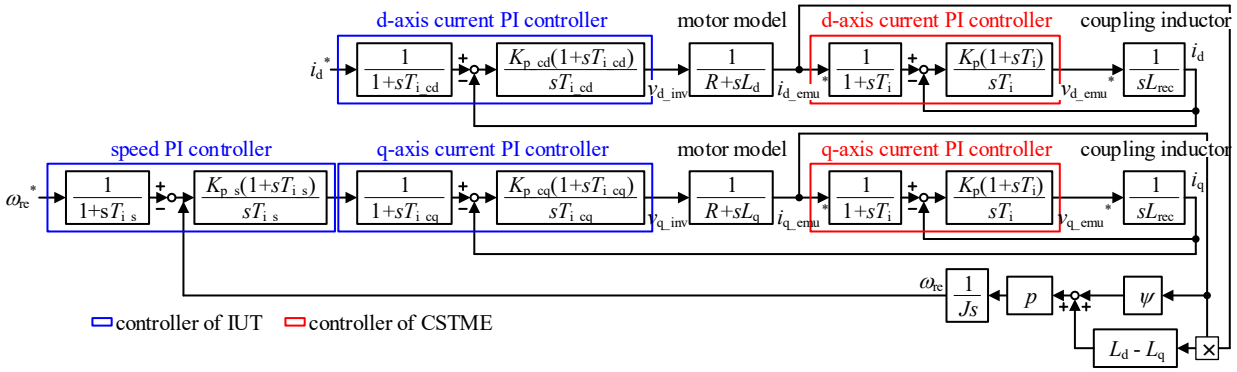

Fig. 3 The control block diagram of the inverter test system with the IUT and the CSTME.

Fig. 3 shows the control block diagram of the inverter test system with the IUT and the CSTME. Note that the Field Oriented Control (FOC) is applied in the IUT. The decoupling control, which is commonly utilized for the IPMSM in order to cancel the cross-coupling terms between the d-axis and the q-axis, is also applied to the IUT. As shown in Fig. 3, the current control loop of the CSTME is put into the current control loop of the IUT. Thus, the system might become unstable due to the interference between each current controller when the bandwidth of both current controllers is dose.

Fig.4 shows the block diagram of the current controller used in the CSTME. The transfer function of the PI current controller used in the CSTME is expressed as

$$G_{PI}(s) = K_{\mathrm{p}} \frac{1+sT_{\mathrm{i}}}{sT_{\mathrm{i}}} \quad \text{.....(5),}$$

where K_{p} is the proportional gain, and T_{i} is the integral time. The closed-loop transfer function of the inductor current controller is expressed as

$$G_{\mathrm{c}}(s) = \frac{\frac{K_{\mathrm{p}}}{L_{\mathrm{rec}}T_{\mathrm{i}}}(1+sT_{\mathrm{i}})}{s^2 + \frac{K_{\mathrm{p}}}{L_{\mathrm{rec}}}s + \frac{K_{\mathrm{p}}}{L_{\mathrm{rec}}T_{\mathrm{i}}}} \quad \text{.....(6).}$$

The first-order lag element is inserted into the current command in order to cancel the zeros of the controller. The first-order lag element F(s) is expressed as

$$F(s) = \frac{1}{1+sT_{\mathrm{i}}} \quad \text{.....(4).}$$

The parameters of the controller K_{p} and T_{i} are designed by comparison with the second-order standard form. The second-order standard form is represented as

$$G(s) = \frac{\omega^2}{s^2 + 2\zeta\omega s + \omega^2} \quad \text{.....(7),}$$

where ω is the natural angler frequency and ζ *i*s the damping factor, which is set to 0.707. The parameters of the PI controllers are calculated by (8) and (9).

$$K_{\mathrm{p}} = 2\zeta\omega L_{\mathrm{rec}} \quad \text{.....(8).}$$

$$T_{\mathrm{i}} = \frac{2\zeta}{\omega} \quad \text{.....(9).}$$

In this paper, the required current control bandwidth f_{c} is clarified by stability analysis. The relationship between ω and f_{c} is expressed as

$$\omega = 2\pi f_{\mathrm{c}} \quad \text{.....(10).}$$

III. Stability Analysis

In this section, the stability of the motor emulation system is analyzed by the system's pole arrangement.

Table 1 shows the parameters of the MUT in this paper. Two types of motors are used to evaluate the stability of the controller.

A. Ideal model

Fig. 5 shows the simplified block diagram analyzed in this paper. Table 2 shows the parameters used in the analysis. The ideal model neglects the control delay, parameter mismatching, out voltage error of power converters, current detection error, and so on.

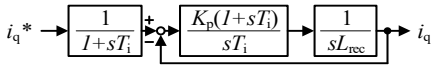

Fig. 4 Configuration of the current PI controller.

Table 1 The parameters of the target IPMSM.

(a) Motor A.

Parameter	Symbol	Value
Output power	P_{n}	3.7 kW
Maximum speed	ω_{n}	7200 rpm
Output torque	T_{n}	4.91 N·m
Pole pairs	p	2
Winding resistance	R	116 mΩ
d-axis inductance	L_{d}	2.59 mH
q-axis inductance	L_{q}	3.63 mH
flux linkage of permanent magnet	Ψ_{m}	0.0905 Wb
Moment of inertia	J	30×10^{-4} N·m

(b) Motor B

Parameter	Symbol	Value
Output power	P_{n}	5.5kW
Maximum speed	ω_{n}	1500rpm
Output torque	T_{n}	35N·m
Pole pairs	p	3
Winding resistance	R	0.21Ω
d-axis inductance	L_{d}	4.3mH
q-axis inductance	L_{q}	10.2mH
flux linkage of permanent magnet	Ψ_{m}	0.2001 Wb
Moment of inertia	J	18×10^{-3}N·m

The zero-d-axis-current control is applied to the IUT. The block diagram shown in Fig. 5 is expressed as only the q-axis controller because the effect of the d-axis disappears with the feed-forward compensation of the cross-coupling terms and the zero-d-axis-current control. The system stability is analyzed based on the simplified block diagram shown in Fig. 5.

Fig. 6 shows the root locus of the whole system when the current control bandwidth of the CSTME which is represented as $f_{\mathrm{c\_emu}}$ is varied from 900 Hz to 1100 Hz for analysis on motor A and motor B. The pole arrangement of the system is calculated by MATLAB/Simulink. Note that the current control bandwidth of the IUT which is represented as $f_{\mathrm{c\_inv}}$ is set to 500 Hz at a constant. As shown in Fig. 5, the poles are shifted to the left half plane (LHP) according to increasing the bandwidth of the current controller in the CSTME. The poles are placed in the right half plane (RHP) when the current control bandwidth of the CSTME is less than or equal to 1032 Hz in Fig. 5 (a) (Motor A) and 1055 Hz in Fig. 5 (b) (Motor B). This means that the stability limits of the systems with motor A and Motor B are 1033 Hz and 1055 Hz, respectively. The stability limits of the two systems become almost the same even the Motor A and Motor B have different power and speed rating. It means that the stability limit is robust for the motor parameters.

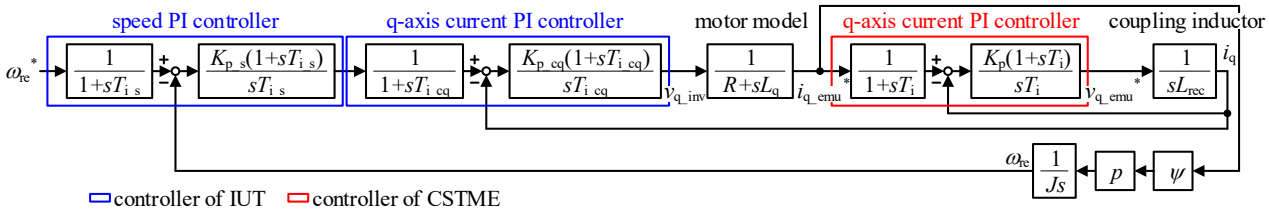

Fig. 5 The simplified control block diagram of the CSTME and the IUT with FOC.

Fig. 7 shows the relationship between the current control bandwidth of the IUT and the CSTME when the system is at the stability limit. The current control bandwidth of the IUT is varied from 100 Hz to 1000 Hz. As shown in Fig. 7, the current control bandwidth of the CSTME at a stable limit is changed almost linearly according to the bandwidth of the IUT. In any case, the bandwidth of the CSTME at a stable limit is approximately 2.1 times higher than the bandwidth of the IUT. Therefore, the current controller of the CSTME requires 2.2 times higher bandwidth than the current control bandwidth of the IUT in order to keep the system stability.

B. Including time delay element model

An actual system has a time delay, which is caused by sampling, PWM, detection, and so on. These delays have a significate influence on the system's stability [15]-[16]. The time delay is assumed as one sampling time by the DSP in this paper. Then, the transfer function $G_d(s)$ of the time delay element is expressed as

$$G_d(s)=\frac{1}{1+T_s s} \quad \text{..... (11)},$$

where T_s is the sampling time, which is the inverse of the switching frequency shown in Table 2. Note that the delay times T_s of the IUT and the CSTME are represented as T_{s_inv} and T_{s_emu}, respectively.

Fig. 8 shows the system block diagram considering the time delay element. The PWM delays are added to the PI controller of both current controllers. The first-order lag element is connected to the output part of the IUT and the CSTME, respectively.

Fig. 9 shows the root locus of the whole system considering the PWM delay when the current control bandwidth of the CSTME is varied from 1150 Hz to 1450 Hz for analysis. The current control bandwidth of the IUT is set to 500 Hz at a constant, as well as the ideal analysis. As shown in Fig. 9, the poles are shifted to the LHP according to increasing the bandwidth of the CSTME, as well as the ideal model analysis results. The poles are placed in the RHP when the current control bandwidth of the CSTME is less than or equal to 1277 Hz in Fig. 5 (a) (Motor A) and 1302 Hz in Fig. 5 (b) (motor B). This means that the stability limits of the systems are 1277 Hz and 1302 Hz, respectively. The stability limit of the including time delay model becomes approximately 1.24 times higher than that of the ideal model. Besides, the system stability limit becomes almost same regardless of the motor parameters in this case.

Fig. 10 shows the required current control bandwidth of the CSTME for Motor A. The vertical axis represents a ratio to the current control bandwidth for the IUT. Fig. 10 (a) shows the required bandwidth of the CSTME when the sampling time delay T_s is not included. The required

Table 2 Analysis Parameters.

Parameter	Symbol	Value
Coupling inductor	L_{rec}	1.73mH
ASR bandwidth of IUT	f_{s_inv}	20 Hz
ACR bandwidth of IUT	f_{c_inv}	500 Hz
IUT switching frequency	f_{sw_inv}	20 kHz
CSTME switching frequency	f_{sw_rec}	100 kHz

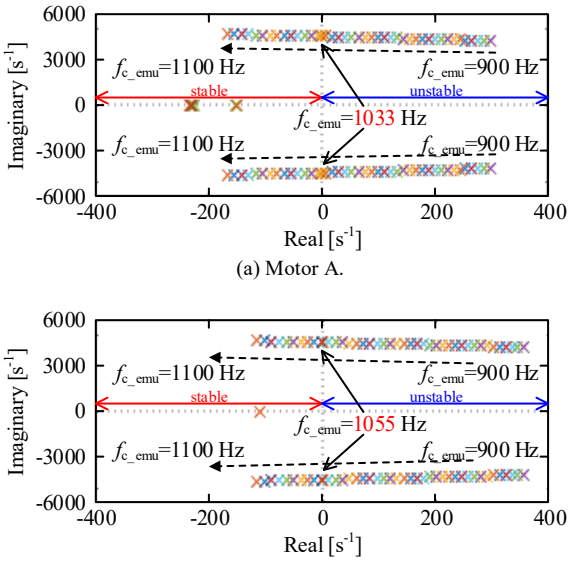

(a) Motor A.

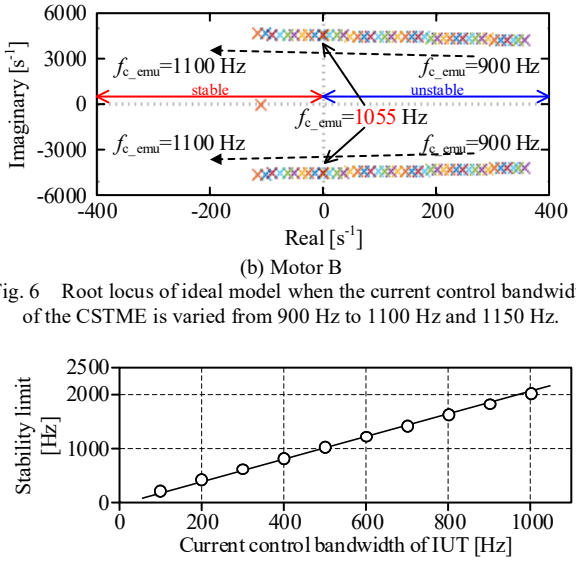

(b) Motor B

Fig. 6 Root locus of ideal model when the current control bandwidth of the CSTME is varied from 900 Hz to 1100 Hz and 1150 Hz.

(a) Motor A.

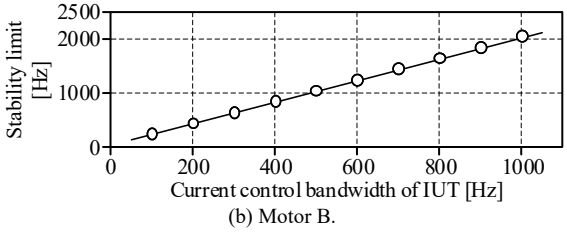

(b) Motor B.

Fig. 7 Stability limit of the ideal model when the current control bandwidth of IUT varied from 100 Hz to 1000 Hz.

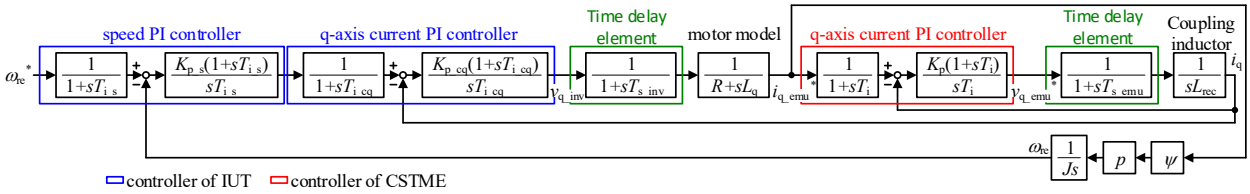

Fig. 8 Control block diagram of the CSTME and the IUT with the delay time element.

bandwidth is 2.2 times of the current control bandwidth of the IUT when the bandwidth of the IUT is set to from 400 Hz to 1000 Hz. The ratio of required bandwidth for the CSTME is increased when the bandwidth of the IUT is set to 400 Hz or less. The reason is to maintain the current PI control for coupled inductor that fast for the electrical time constant of the motor model. On the other hands, Fig. 10 (b) shows the required current control bandwidth of the CSTME with the sampling delay T_{s_inv} and T_{s_emu}. Then, the ratio of required bandwidth of the CSTME is increased. As a result, the required bandwidth becomes more than 3.1 times of the current control bandwidth of the IUT when that of the CSTME is less than 1000 Hz.

Fig. 11 shows the difference of the pole placement between with and without time delay in same bandwidth. The current control bandwidth of the CSTME is set to 1200 Hz and 1300 Hz when the IUT's current control bandwidth is 500 Hz. All the poles are in the LHP and the system is stable under both bandwidth in the model without time delay. In contrast, poles are in the RHP when the current control bandwidth of the CSTME is set to 1200 Hz in the model with time delay. Thus, the system is more unstable due to the effect of the time delay, even in the same current control bandwidth.

IV. Simulation Results

This section verifies the validity analysis in section III on the time domain. The PLECS (Plexim) is used for the verification. The current control bandwidth of the IUT is set to 500 Hz. A ramped speed command is given in order to accelerate in the rated acceleration time of the MUT (Motor A). After the end of acceleration, the step torque supplies to the CSTME or the IPMSM from 0 Nm to 4.91 Nm (rated torque).

Fig. 12 shows the CSTME responses with and without the time delay when the current control bandwidth of the IUT is set to 500 Hz. The oscillation of torque and q-axis current increase when the current control bandwidth of the CSTME is 1032 Hz with the time delay and 1276 Hz without the time delay although the oscillations decrease when the current control bandwidth of the CSTME is 1033 Hz in (a) and 1077 Hz in (b). The stability limit becomes from Fig. 12 (a) and (b), the results of the stability limit agree with the root locus analysis in Section III, respectively. From these results, the stability analysis is verified.

Fig. 13 shows the difference in the CSTME responses between with and without the time delay when the current control bandwidth of the CSTME is set to 1300 Hz. As shown in Fig. 11, the system is stable with and without delay time when the current control bandwidth of the

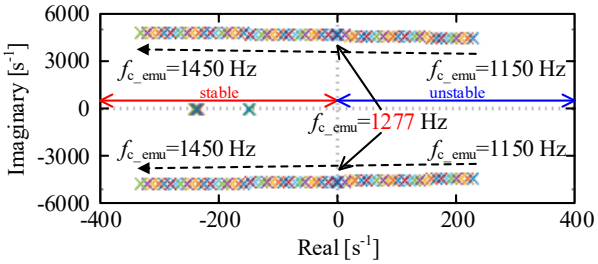

(a) Motor A.

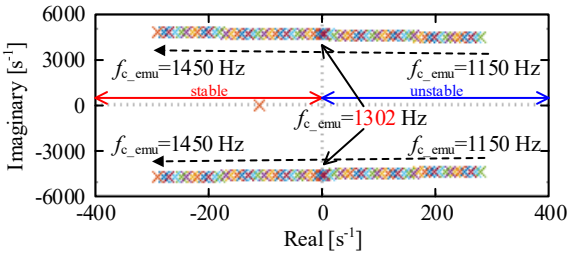

(b) Motor B

Fig. 9 Root locus of model with time delay when the current control bandwidth of the CSTME is varied from 1150 Hz to 1450 Hz.

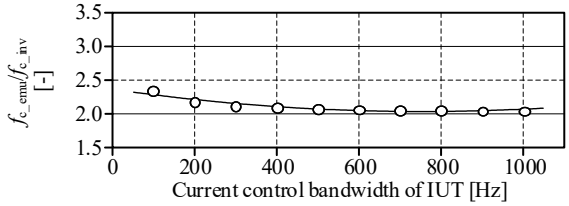

(a) Without time delay.

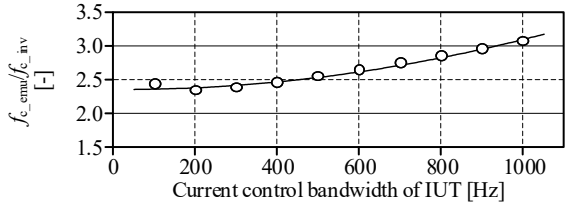

(b) With time delay.

Fig. 10 Stability limit of the model with and without time delay when the current control bandwidth of IUT varied from 100 Hz to 1000 Hz (Motor A).

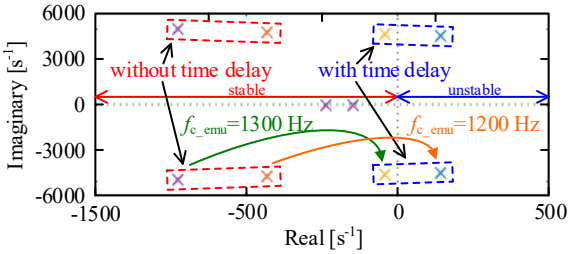

Fig.11 The difference of pole placement between with and without time delay in same bandwidth. The current control bandwidth of CSTME is set to 1200 Hz and 1300 Hz (Motor A).

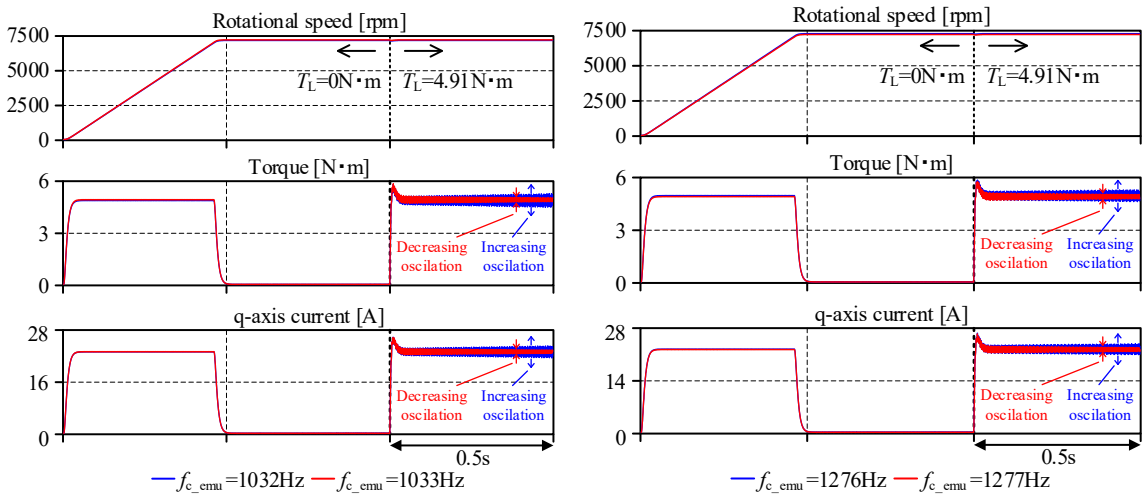

(a) Without time delay. The stability limit is between 1032 Hz and 1033 Hz. (b) With time delay. The stability limit is between 1276 Hz and 1277 Hz.

Fig.12 CSTME response when the bandwidth of the current controller is near to stability limit (Motor A).

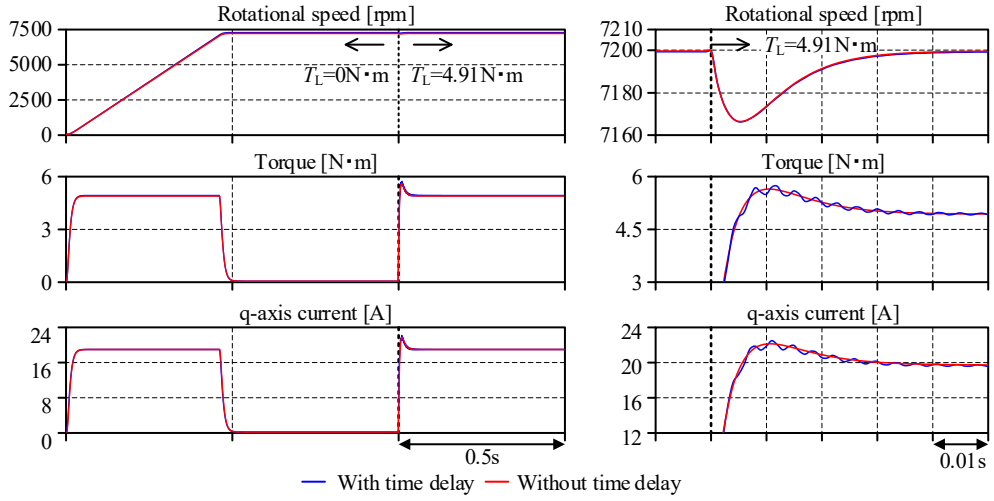

Fig.13 The difference of CSTME responses between with and without time delay when the current control bandwidth of CSTME is set to 1450 HZ (Motor A).

CSTME is 1300 Hz. However, the oscillations occur only when there is the delay time. No oscillation occurs because the dominant poles, which are the closest pole to RHP, are on the real poles when there is no the delay time, as shown in Fig. 11. In contrast, the complex conjugate pole becomes the dominant pole when there is the delay time. Thus, the response becomes oscillatory. Then, the occurrence of such oscillations in the motor drive testing is unacceptable. Therefore, the design of the current control bandwidth for the CSTME must not only satisfy the stability limits of the system, but also ensure that the imaginary part poles should be located at that point, where if far from the real part poles.

Fig.14 shows the responses of the IPMSM (Motor A) and the CSTME at stable conditions. The current control bandwidth of the IUT and the CSTME are set to 500 Hz and 2000 Hz, respectively. A comparison of the amount of overshoot that occurs after a torque step agrees within an error of 4 % or less. Thus, the CSTME imitates the IPMSM with accuracy. This error is minimized by reducing the integration time of the current PI controller of the coupling inductor. This means that the accuracy of the imitation is improved by increasing the current control bandwidth of the CSTME. In addition, the delay time is considered to affect the response of the PI controller. However, the overshoot is almost same with and without the delay time. This is because the electrical time constant of the motor is sufficiently slow compared to the response of the PI controller.

V. Conclusions

This paper derives the required current control bandwidth of the CSTME to prevent system instability. The system stability with and without the sampling delay was also analyzed using a root locus. From the analysis result, the current controller of the CSTME required 2.2 times higher bandwidth than the IUT's bandwidth in the ideal conditions. On the other hands, when the sampling delay is included, the required bandwidth of the CSTME becomes more than 3.1 times when the IUT's current control bandwidth of less than 1000 Hz.

The future works are the following, analysis with more rigorous models considering discretization, etc.; experimental verification of stability under different conditions such as coupling inductors, switching

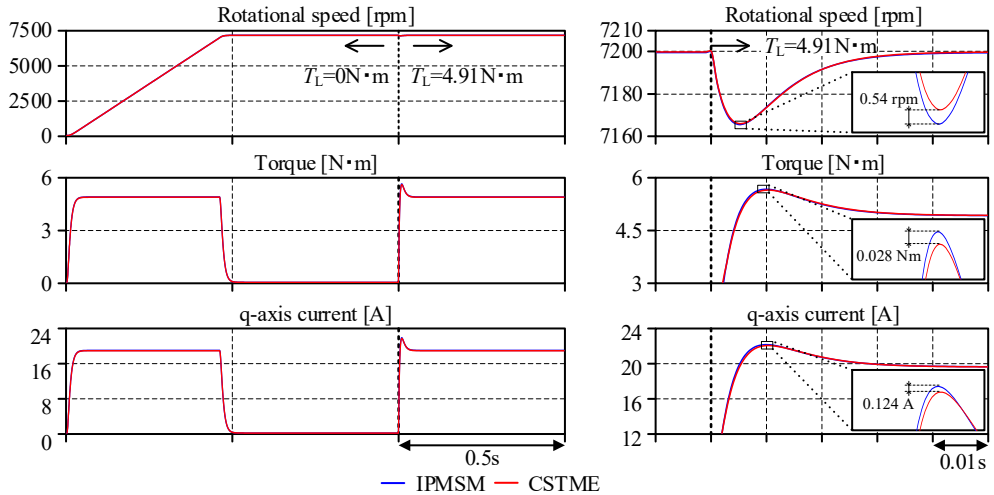

(a) Without time delay.

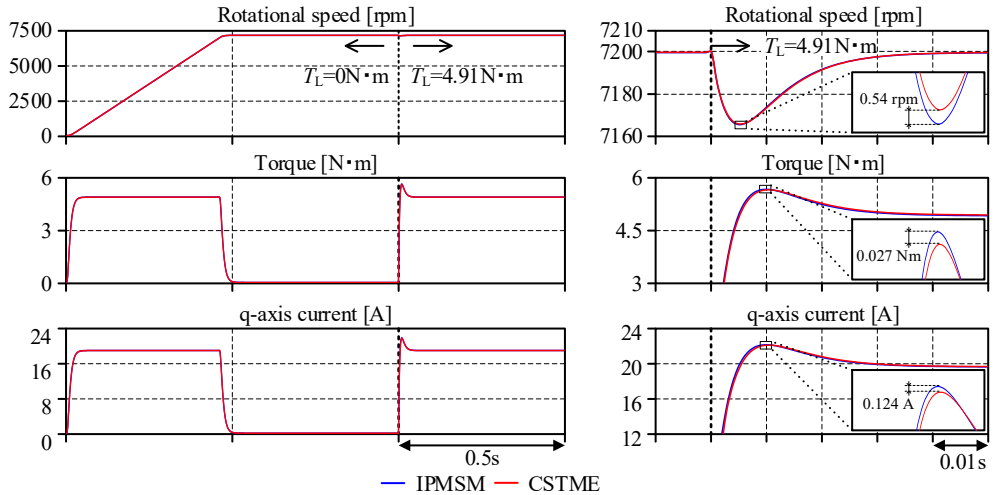

(b) With time delay.

Fig.14 IPMSM and CSTME responses at stable conditions. The delay time of CSTME T_{s_emu} and the integral time T_i are 10 μs and 113 μs in this condition, respectively (Motor A).

frequency, and so on; consideration of a method to achieve fast current response for higher performance of the CSTME.

REFERENCES

[1] A. Bouscayrol, “Different types of Hardware-In-the-Loop simulation for electric drives”, in IEEE International Symposium Industrial Electronics, Cambridge, UK, 2008, pp. 2146-2151.

[2] Miao Hong, Yushi Miura, Toshifumi Ise, Yuki Sato, Toshifumi Momose, and Christian Dufour, “Stability and Accuracy Analysis of Power Hardware-in-the-loop Simulation of Inductor Coupled systems”, in IEEJ Transaction of Industry Applications, vol. 130, No. 7, 2010.

[3] Miao Hong, Satoshi Horie, Yushi Miura, Toshifumi Ise, Yuki Sato, Toshinari Momose, and Christian Dufour, “Power Hardware-in-the-loop Simulation of a Gas Ensine Cogeneration System for Development a Power Converter System”, in IEEJ Transaction of Industry Applications, vol. 130, No. 5, 2010.

[4] Shizunori Hamada, Toshimichi Takahashi, Nobutaka Kezuka, Masaju Kouketsu, and Shingo Ishigaki, "Inverter Drive of Dynamometers for Automotive Evaluation System", in Proc. Int. Power Electron. Conf., 2018, pp. 227–232.

[5] Kenichiro Saito, and Hirofumi Akagi, “A Power Hardware-in-the-Loop (P-HIL) Test Bench Using Two Multilevel DSCC Converter for a Synchronous Motor Drive”, in IEEE Transaction on Industry Applications, Vol. 54, No. 5, September/October 2018.

[6] K. Saito and H. Akagi, “A Real-Time Emulator of a Medium-Voltage High-Speed Induction Motor Loaded With a Centrifugal Compressor”, in IEEE Transactions on Industry Applications, vol. 55, no. 5, pp. 4821–4833, September/October 2019.

[7] Kenichiro Saito, and Hirofumi Akagi, “A Real-Time Real-Power Emulator for a Medium-Voltage High-Speed Electrical Drive: Discussion on Mechanical Vibrations”, in IEEE Transaction on Industry Applications, Vol. 57, No. 2, March/April 2021.

[8] Nimananda Sharma, Georgios Mademlis, Yujing Liu, and Junfei Tang, “Evaluation of Operating Range of a Machine Emulator for a Back-to-Back Power-Hardware-in-the-Loop Test Bench”, in IEEE Transaction on Industrial Electronics, Vol. 69, No. 10, October 2022.

[9] Ke Ma, and Yubo Song, “Power-Electronic-Based Electric Machine Emulator Using Direct Impedance Regulation”, in

IEEE Transaction on Power Electronics, Vol. 35, No. 10, October 2020.

[10] Mohammad A. Masadeh, K. S. Amitkumar, and Pragsen Pillay, "Power Electronic Converter-Based Induction Motor Emulator Including Main and Leakage Flux Saturation," in IEEE Transaction on Transportation Electrification, vol. 4 no. 2, June 2018.

[11] Visweshwar Chandrasekaran, Benjamin Sykora, Sanchit Mishra, and Ned Mohan, "A Novel Model Based Development of a Motor Emulator for Rapid Testing of Electric Drives," in 2020 Energy Conversion Congress and Exposition (ECCE), 2020, pp. 2395-2402.

[12] Fletcher E. Fleming, and Chris S. Edrington, "Real-Time Emulation of Switched Reluctance Machines via Magnetic Equivalent Circuits," in IEEE Transaction on Industrial Electronics, vol. 63, no. 6, June 2016.

[13] K. S. Amitkumar, R. Sudharshan Kaarhik, and Pragasen Pillay, "A Versatile Power-Hardware-in-the-Loop-Based Emulator for Rapid Testing of Transportation Electric Drives," in IEEE Transaction on Transportation Electrification, vol. 4, no. 4, December 2018.

[14] Lei Zhu, Dong Jiang, Ronghai Qu, Leon M. Tolbert, and Qiao Li, "Design of Power Hardware-in-the-Loop Simulations for Integrated Starter-Generator Systems," in IEEE Transaction on Transportation electrification, vol. 5, no. 1, March 2019.

[15] Yuanhao Xie, Dong Jiang, and Zicheng Liu, "Improved Accuracy of Power Electronic-Based Motor Emulation With Compensation for Signal Transmission Delay", in IEEE Transactions on Transportation Electrification, Vol. 8, on. 1, March 2022.

[16] Hiroki Takahashi, and Jun-ichi Itoh, “Control Method for a Matrix Converter to Ensure Compatibility between Filter Resonance Suppression and Output Current Control Performance”, in IEEJ Transaction on Industry Applications, Vol. 135, No. 7, pp. 802-815, 2015.